Science of the Total Environment 696 (2019) 134062

Contents lists available at ScienceDirect

Science of the Total Environment

journal homepage: www.elsevier.com/locate/scitotenv

Land use interacts with changes in catchment hydrology to generate chronic nitrate pollution in karst waters and strong seasonality in excess nitrate export

Fu-Jun Yue [a,b], Susan Waldron [a], Si-Liang Li [b,*], Zhong-Jun Wang [c], Jie Zeng [c], Sen Xu [b], Zhi-Cai Zhang [d], David M. Oliver [e]

[a] School of Geographical and Earth Sciences, University of Glasgow, Glasgow G12 8QQ, United Kingdom
[b] Institute of Surface-Earth System Science, Tianjin University, Tianjin 300072, China
[c] State Key Laboratory of Environmental Geochemistry, Institute of Geochemistry, Chinese Academy of Sciences, Guiyang 550081, China
[d] State Key Laboratory of Hydrology–Water Resources and Hydraulic Engineering, Hohai University, Nanjing 210098, China
[e] Biological & Environmental Sciences, Faculty of Natural Sciences, University of Stirling, Stirling FK9 4LA, United Kingdom

HIGHLIGHTS

- Sensor technology in the karst critical zone offers high resolution NO_3^- dynamics.
- Hydrological and seasonal NO_3^- responses were observed at multiple spatial scales.
- NO_3^- export varied by season in response to sources availability and karst aquifer.
- Sensor technology revealed chronic aquifer NO_3^- pollution.

GRAPHICAL ABSTRACT

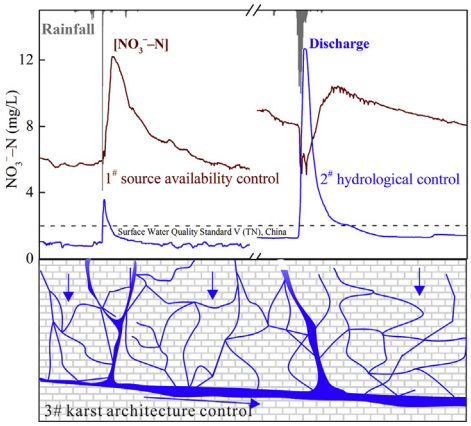

ARTICLE INFO

Article history:
Received 4 June 2019
Received in revised form 19 July 2019
Accepted 21 August 2019
Available online xxxx

Editor: José Virgílio Cruz

Keywords:
Chronic nitrate pollution
Karst critical zone

ABSTRACT

Agricultural land in karst systems can pollute water courses, with polluted waters travelling quickly to and through the sub-surface. Understanding how rapidly nitrate moves within the highly-transmissive karst critical zone (from soils to aquifers) is limited by low resolution data. To understand nitrate behavior and its controls, we deployed sensor technology at five sites to generate autonomously high-resolution time series of discharge and NO_3^-–N, which is the major nitrogenous component, in a farmed karst catchment in Southwestern China. The [NO_3^-–N] time series exhibited rapid response to rainfall-induced increases in discharge and a large magnitude in [NO_3^-–N], from 0.72 to 16.3 mg/L across five sites. However, the magnitude of NO_3^-–N response at each site was varied during rainfall events (wet season) and dry season. The highest mean [NO_3^-–N] and normalized annual fluvial export occurred in a headwater catchment with a developed karst aquifer system. Seasonal variation in NO_3^-–N export occurred in response to source availability, most notable in catchments with valley agriculture: in the wet season up to 94% of nitrate was exported from the headwater catchments within two months, but at

* Corresponding author.
E-mail address: siliang.li@tju.edu.cn (S.-L. Li).

https://doi.org/10.1016/j.scitotenv.2019.134062

Nitrate sensor
Nitrate export

the larger catchment scale, over the 6 month wet season, only 61% of total export occurred. At the larger catchment scale, [NO_3^-–N] were lower due to buffering by the karstic aquifer network. From the time series we observe little decrease in [NO_3^-–N] as discharge decreases in the dry season, indicating the karst aquifers are chronically-polluted with nitrate through slow flow pathways.

1. Introduction

Nitrate (NO_3^-) contamination of surface and ground waters is a worldwide concern; it can impact on the ecological quality of aquatic environments and pose a risk to human health if drinking water is contaminated (Van Meter et al., 2017; Zhang et al., 2015). Agricultural activities dominate nitrogen (N) delivery to aquatic systems when excessive N fertilizer application exceeds the plant growth requirements (Coxon, 2011; Lassaletta et al., 2014). This scenario is particularly likely in rapid response aquifers, such as those in karst, an important landscape covering approximately 20% of the Earth's ice-free continent area and supplying drinking water for 25% of the world's population (Ford and Williams, 2013; Hartmann et al., 2014). Karst soils are thin, patchy, fragile and slow to form, thus the limited farmland area in karst regions is important for food production and requires careful management to prevent further deterioration of the karst ecosystem (Buckerfield et al., 2019; Coxon, 2011; Jiang et al., 2009).

The karst aquifer structure is characterized by conduit, fracture and matrix flow resulting in fast (e.g. conduit) and slow (e.g. fracture and matrix) flow pathways (Ford and Williams, 2013; Hartmann et al., 2014). The relative proportions of two flows will influence discharge and contaminant distribution. Where karst hosts agricultural land, evaluating nitrate transfer and attenuation from soil into groundwater i.e. through the critical zone, is a challenge that must be addressed as the following impacts have been observed: i) contaminants can rapidly be transported from surface to groundwater through sinkholes and fracture networks within the karst architecture (Hartmann et al., 2014; McCormack et al., 2016), yet ii) there are also areas where contaminants can accumulate and act as a 'legacy' source over time (Fenton et al., 2017); iii) the prevalence of rapid transit through the karst aquifer shortens contaminant residence time, reducing capacity for attenuation and affecting receiving water quality (Einsiedl et al., 2009; Katz et al., 2001). For catchment management and better water quality, we need to understand the driving factors and dynamics of nitrate loading to rivers in karst systems. Nitrate loading is a measure of excess nitrogen in the critical zone and should be considered as mass of fluvial nitrate-N (NO_3^-–N) exported, as this indicates better total NO_3^-–N losses.

Hydrological models underpin contaminant models, such as those required for NO_3^-–N movement. But models for karst systems face a further challenge of how to capture spatial heterogeneity (Hartmann et al., 2014). Manual sampling is resource intensive and so this approach to data generation is unlikely to capture the rapid changes in fluvial NO_3^-–N concentrations required to generate an accurate estimate of the nitrate export budget (Blaen et al., 2016). In-situ monitoring, such as using nitrate ion-selective electrodes (ISE), offers higher temporal resolution measurements and a further reduction in uncertainty of trends in export. Sensors have proven less-costly and labor intensive than field sampling and can enable a better understanding of the interaction between concentration and pathways with flow, temperature and other factors (Pellerin et al., 2012; Pu et al., 2011; Rode et al., 2016).

The objectives of this research were to generate high-resolution time series of nitrate-N concentration ([NO_3^-–N]), and from this understand NO_3^-–N behavior and its controlling factors in a karst critical zone (KCZ). Southwestern (SW) China was chosen for this research as it is one of the largest globally continuous karst areas, covering ~5.40 $\times 10^5$ km^2 and it has been proposed the problem of N pollution is so severe that nutrient vulnerable zones should be designated (Bai et al., 2018; Yue et al., 2018). Indeed NO_3^-–N in karst waters was the major dissolved N species, accounting for 85% of the total dissolved N and can be above the drinking water standard of the World Health Organization (50 mg/L as NO_3^-) during the wet season (Liu et al., 2006; Yue et al., 2018). People in these karst areas depend on the local water and so understanding catchment drainage N-loading is important (Liu et al., 2016). In the karst system, underground streams are crucial to surface water quality as they are a source of emergent water. Thus in a typical subtropical karst agricultural catchment, we deployed sensor-technology at five sites comprising four upwelling underground stream sites and one surface stream site to: (1) generate time series of [NO_3^-–N] at KCZ; (2) elucidate how the KCZ influences nitrate response at different spatial and temporal scales; (3) calculate NO_3^-–N exports from the KCZ; (4) identify the primary controlling factors (e.g., nitrate availability, aquifer characteristics, land use) on nitrate export.

2. Materials and methods

2.1. Site description

Our KCZ observatory is the Houzhai Catchment (Fig. 1a), located in Guizhou Province, SW China, with a drainage area of 73.4 km^2 and characterized by subtropical monsoon climate (Zhang et al., 2017). The mean annual temperature is 20.1 °C. The geology comprises mid-Triassic Period limestone and dolomite across the basin. This catchment has been studied since 1978 as a representative cone and cockpit karst geomorphology (Yang, 1981). The geomorphology changes from peak clusters (Liu et al., 2004) with many depressions and bare rock in the upper reaches to peak forests with valleys in the middle reaches, and to extensive plains in the lower reaches of the catchment (Wang and Zhang, 2001).

The steep hillslopes in the east are covered with very thin soil (<0.4 m), discontinuous limestone soil and yellow soil (Liu et al., 2016). The plain area in the west is covered with paddy soil. Using ArcGIS 10.0, we characterized vegetated land use for 2016 in Houzhai Catchment (Fig. 1b). Natural vegetation coverage (45.1%) is highest in the uncultivated steeper mountains, and agriculture (41%) is dominant in the cultivated depressions, including 27.1% rice-rape rotation in paddy fields and 72.9% corn-rape rotation in dry lands (Fig. 1b). Other land cover within the catchment are water (1.4%), bare rock (1.4%), and roads, settlements and small industry (11.1%) (Table S1). Animal waste such as cattle and pig manure are seasonally applied as a fertilizer at the beginning of major crop tillage periods, typically for rape (November, winter crop) and rice (May, summer crop) (Fig. 2). Synthetic fertilizers, urea and diammonium phosphate are also applied (Feng et al., 2009).

Water from two sources, the underground stream upwelling at Maoshuikeng (MSK) and Houzhai surface River (HZ-R), regulated by Qingshan Reservoir (QS-Re) (Fig. 1a), mix downstream and account for >95% of the total discharge of the catchment (Chen et al., 2005). There is another reservoir, the Muzudong Reservoir, (MZD-Re, expanded in 2016) in the upper reaches of catchment (Fig. 1a). The primary underground conduit in the south of the catchment originates from the hilly upper reaches where most surface and underground flow recharges the conduit through sinkholes (Wang and Zhang, 2001; Zhang et al., 2017). The conduit is continuous through the relatively flat plain of the middle and lower reaches and discharges at MSK. The underground conduit in this KCZ is well-developed and connects numerous larger fractures, particularly in upper reaches. Single conduits with characteristically few tributaries are found in the upper

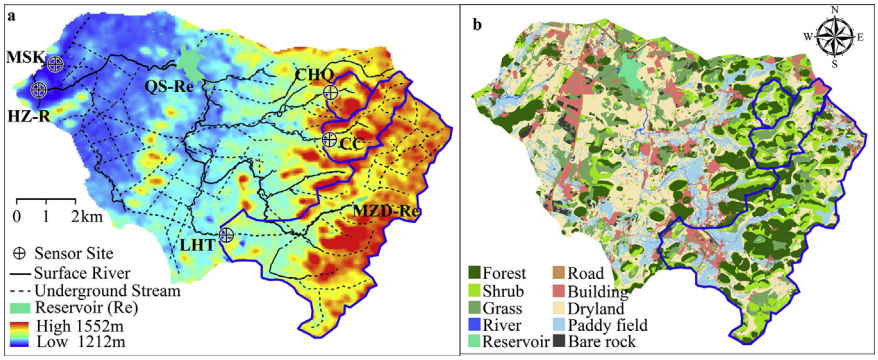

Fig. 1. (a) Topographic and hydrological flow pathways, and observation stations: Chenqi (CHQ), Changchong (CC), Laoheitan (LHT), Maoshuikeng (MSK) and Houzhai River (HZ-R). There are two reservoirs in the catchment, Muzudong (MZD-Re) and Qingshan (QS-Re) (b) Land use in 2016 in the Houzhai Catchment. Three blue dashed line areas represent the surface catchment area of CHQ, CC, and LHT surface catchments. (For interpretation of the references to color in this figure legend, the reader is referred to the web version of this article.)

reaches of catchment (most influencing sites Changchong (CC), Chenqi (CHQ) and Laoheitan (LHT), Fig. 1a) whilst aquifer networks with complex matrix fissures are present in the lower reaches of the catchment (Wang and Zhang, 2001). The spatial heterogeneity of permeability leads to the spatial variation in baseflow to total stream flow (baseflow index), which increases from upper reaches (7.3%) to middle (41.4%) and downstream (84.6%) (Zhang et al., 2016).

Five monitoring sites across the whole catchment were chosen on the basis of land use, catchment scale and the karst aquifer network. For headwater catchments, we chose Chenqi underground stream (CHQ) located in the farmed valley bottom surrounded by forest, and Changchong underground stream (CC) located in shrubs downslope of farmland, but not in the valley bottom (Fig. 1b). To understand whether nitrate loading was attenuated within different catchment scales we chose Laoheitan underground stream (LHT) in the middle reaches, and in the lower reaches MSK and HZ-R at the catchment outlet. Catchment area and land use information for each catchment is detailed in Tables 1 and S1.

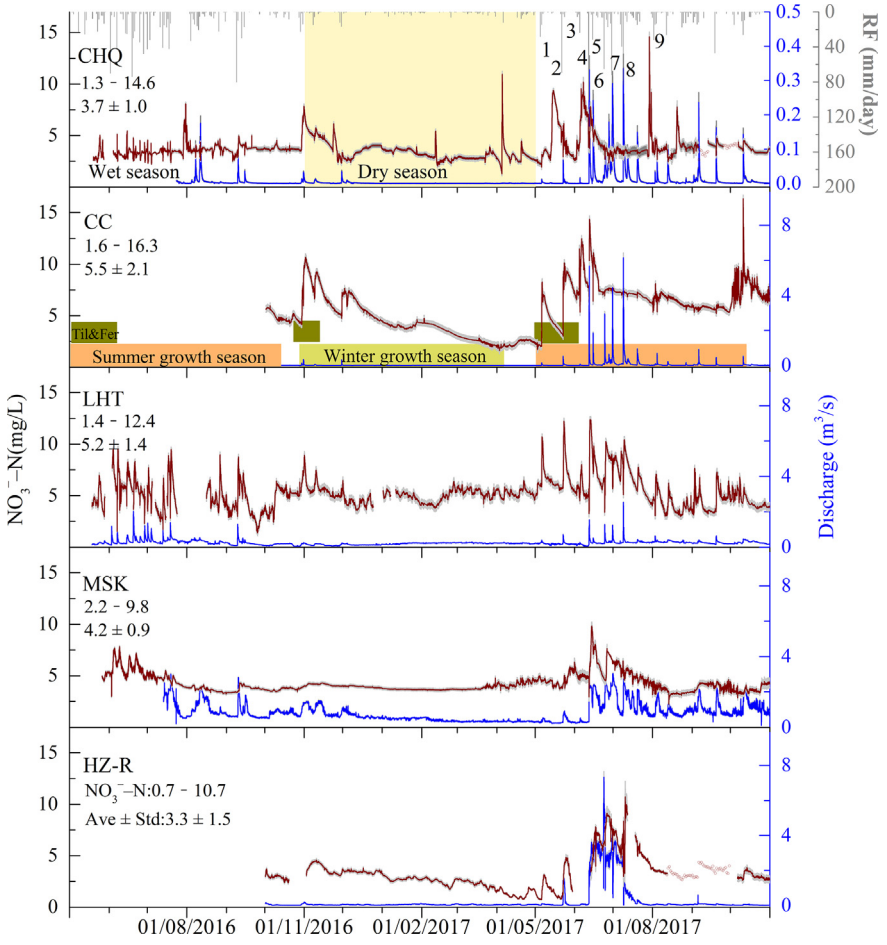

Fig. 2. The time series of in-situ [NO_3^-–N] and Q at the five sites. The shaded gray area associated with [NO_3^-–N] and Q represents the uncertainty of calibration. The light-yellow area represents the dry season (shown for CHQ but relevant for all sites). Gaps in the continuous record indicate missing data. To show the discharge clearly, wet season rainfall events have been numbered and the discharge scale at CHQ is smaller than other sites. Similarly, rainfall (RF), although measured at only LHT is only shown on the first time series. The abbreviations of Til and Fer in CC mean tillage and fertilization, respectively. The color shading in CC shows the time schedule of major agricultural activities across this KCZ. (For interpretation of the references to color in this figure legend, the reader is referred to the web version of this article.)

Table 1
Annual loading and seasonal contribution of NO_3^-–N export.

Sites	Catchment area	Annual loading	Dry season	Wet season	Normalized catchment area loading	Normalized agricultural area loading
	ha	kg	%	%	kg/ha	kg/ha
CHQ	125	$8.75 \pm 1.73 \times 10^2$	9.0	91.0	7.0 ± 1.4	42.1 ± 8.3
CC	319	$9.63 \pm 0.77 \times 10^3$	4.1	95.9	30.2 ± 2.4	116 ± 9.3
LHT	1769	$4.05 \pm 0.26 \times 10^4$	39.4	60.6	22.9 ± 1.5	70.1 ± 4.5
MSK	7339	$10.8 \pm 0.57 \times 10^4$	30.5	69.5	14.7 ± 0.8	35.9 ± 1.9
HZ-R	7339	$5.47 \pm 0.48 \times 10^4$	3.1	96.9	7.5 ± 0.7	18.2 ± 1.6

2.2. High frequency NO_3^-–N monitoring

Severe soil erosion in karst systems can lead to highly-turbid event flow waters, observed here (Coxon, 2011; Peng and Wang, 2012). This could affect the performance of the optical sensors during events, a time period important to capture accurately as nitrate loading may be dynamic (Blaen et al., 2016). Thus, we chose the non-optical NISE sensor, successfully used elsewhere in drinking water and river monitoring (Exner-Kittridge et al., 2016; Tang et al., 2012). Sensors were installed at the CHQ, LHT and MSK site in May 2016 and at CC and HZ-R in October 2016. The sensors were powered by 24 V DC batteries, supplemented by solar panels, and recorded [NO_3^-–N] every 15 min.

Grab samples were manually collected over the duration of the observation period for measurement of [NO_3^-–N], with Cd-reduction to detect nitrate as nitrite by automatic flow analyzer (SKALAR Sans Plus Systems), analytical detection limit of 0.1 mg/L. The laboratory measured concentrations were used to create a calibration for each sensor by linear regression with [NO_3^-–N] recorded by the sensor, and from this a time series could be generated. Across all sites, uncertainty of estimated field [NO_3^-–N] (μ_C) was between 0.02 and 0.64 mg/L. Details of the sensor principle and uncertainty in calibration approach can be found in the Supplementary information (Text S1, Fig. S1 and Table S2).

2.3. Discharge and rainfall

At the same location as the nitrate sensors, Hobo pressure transducers automatically measured water level every 15 min and a stage-discharge relationship was used to produce the discharge (Q) time series (Chen et al., 2018; Zhang et al., 2019). The uncertainty in calculation of discharge (μ_Q) arising from sensor calibration and precision of the pressure-transducer was considered. Rainfall for the catchment is measured at LHT meteorological station, as considered to vary little given the meteorological drivers of rainfall and the catchment size.

2.4. The annual NO_3^-–N loading

Here we report [NO_3^-–N] time series from 18th May 2016 to 31st October 2017 at CHQ, LHT and MSK, and from 1st October 2016 to 31st October 2017 at CC and HZ-R sites. Although the study period captures more than one hydrological year, the annual load of NO_3^-–N was calculated for all five sites from November 2016 to October 2017. [NO_3^-–N] and Q are both available for this period and it captures consecutive and full wet and dry seasons (Fig. S2), while a hydrological year calculation would split the wet season response. The calculated method of annual NO_3^-–N loading and normalized annual NO_3^-–N loading at each site can be found in Text S2 and Table S3.

3. Results and discussion

3.1. Time series of NO_3^-–N concentration at five sites in Houzhai Catchment during study period

Rainfall was distributed throughout the year with approximately 86% of the annual rainfall 1217 mm (Fig. 2), occurring during the wet season (May to October), particularly in June and August, during November 2016 to October 2017 - which had similar rainfall totals and distribution to the average rainfall in a typical year (1246 mm) (Yue et al., 2018). Intensive rainfall events sustained high Q and some rainfall responses in Q overlap (e.g. event 7 at CHQ, Fig. 2). To clearly show the fluvial events, nine major intensive rainfall events during the wet season, often >30 mm within 24 h, with total rainfall 748.6 mm during 5th May and 3rd Aug 2017 were numbered in Fig. 2 and detail information supplied in Table S4.

Across all five sites, [NO_3^-–N] ranged from 0.7 to 16.3 mg/L (Fig. 2). This range in [NO_3^-–N] is wider than observed in other karst systems in Europe and North America, with ranges of 8 and 2.5 mg/L respectively (Fenton et al., 2017; Huebsch et al., 2014; Jost et al., 2011; Musgrove et al., 2016), and much greater than non-karst catchments with agricultural and forest dominating land-use (Jacobs et al., 2018; Miller et al., 2016). However, some sites with narrower ranges had higher mean [NO_3^-–N] that this catchment, for example a small Irish catchment with >90% land use for intensively operated dairy farming (Fenton et al., 2017; Huebsch et al., 2014).

The lowest [NO_3^-–N] was not observed synchronously across sites. For example, minimum [NO_3^-–N] was observed during rainfall events in the wet season at the larger catchment scale (LHT and MSK), likely as a result of dilution. In contrast minimum [NO_3^-–N] in the headwaters and the surface river was observed in the dry season when nitrate availability is low and likely biological demand is greater (Wymore et al., 2016). The maximum [NO_3^-–N] for all sites was observed during the wet season, but also not synchronously at the different catchment scales, indicating different response time, transport processes or efficiency of attenuation (Einsiedl and Mayer, 2006; McMahon and Bolke, 2006). In the headwater (CC), the highest concentration was at the end of wet season during the beginning of the winter crop fertilization period, while in the other headwater catchment, where the site (CHQ) is located in the valley bottom, this occurred three months prior. The highest [NO_3^-–N] in CHQ occurred during low Q (0.75 L/s) indicating this was not hydrologically controlled. High concentration during the dry season was similarly observed in CHQ, so this type of response may represent an incidental loading (Shore et al., 2016). For large catchments, the highest concentrations were observed during rainfall events, e.g. event No. 4 at LHT and MSK, and No. 8 at HZ-R (Fig. 2). Overall, it seems that nitrogen source availability and hydrology determined the occurrence of extremum [NO_3^-–N].

Although the extremum [NO_3^-–N] response varied between sites, the time series of [NO_3^-–N] at all sites demonstrated a clear seasonal variation with more concentration maxima observed in the wet season than dry season. In the dry season, [NO_3^-–N] were generally similar to non-event flow in the wet season, with the surface water (HZ-R) and one headwater catchment (CC) showing a decrease with time. In addition, patterns in [NO_3^-–N] with flow also varied between the catchments. For example, there are [NO_3^-–N] peaks in each catchment in the dry season, but the maximum [NO_3^-–N] at the largest catchment (MSK and HZ-R) was less than other sites.

There was a significant difference in mean [NO_3^-–N] (two-way ANOVA, $p < 0.001$, $\alpha = 0.05$) across different catchment scales and between NO_3^-–N emergence from underground stream and surface flow, suggesting that the nitrate mobilization is varied across catchment

scales, and underground streams and surface streams. Compared to the two headwater catchments, underground streams located in areas with a high proportion of forest cover (CHQ) displayed significantly ($p < 0.001$) lower average [NO_3^-–N], indicating that land use can markedly impact on karst aquifers. Although having a similar proportion of forest (Table S1), the mean [NO_3^-–N] in three underground streams (CC, LHT, MSK) decreased as catchment area increased, suggesting that nitrate leaching in valley bottom agriculture of headwater catchments is greater and nitrate may attenuate within the underground stream (Heffernan et al., 2012; Musgrove et al., 2016; Yue et al., 2018). The relationship between [NO_3^-–N] and Q is far more complex and non-uniform behavior was observed at these sites (Fig. S3), generating wide scatter in the concentration and discharge relationship in headwater catchments with well-developed conduits (CHQ and CC). At three sites we can compare the 2016 and 2017 wet season. Although increases in [NO_3^-–N] in response to event flow are evident in 2016 (total rainfall 1135 mm), the maxima in [NO_3^-–N] are lower and the events are less-clearly defined than in 2017 (1049 mm). The higher intensity via less frequent rainfall events in the 2017 wet season was able to more effectively initiate mobilization which can result in higher concentrations or longer duration of nitrate loading periods.

3.2. NO_3^-–N export from the KCZ

The daily NO_3^-–N loading ranged from 0.07 ± 0.006 to 2635 ± 20 kg (daily loading ± uncertainty) with high NO_3^-–N export occurring during the periods of great Q (Fig. 3). There was a strong relationship between daily NO_3^-–N loading and daily average Q, which was consistent across all sites but all suggested greater loading increases with higher discharges due to greater N export (increase in [NO_3^-–N] as evidenced by the sensors, Fig. 2).

In addition, there were seasonal and across-site differences in the quantity of NO_3^-–N exported, apparent from cumulative N loading curves (Figs. 3 and 4a). Most NO_3^-–N is lost from land to drainage during the wet season, and in event flow, but the proportion of annual NO_3^-–N exported during this period varied between sites (Fig. 4). Sites were classified two types, steep cumulative (CHQ and CC) and linear export (LHT and MSK) which indicated karst critical zone have varied influence on different catchment scales. For example, there is relatively less variation of daily NO_3^-–N loading at large catchment scales, e.g. LHT and MSK, than small catchment (Fig. 3). Further, during the wet months of June to August 36–94% of the total annual NO_3^-–N export took place, with the smallest export at LHT and the largest export at HZ-R (Fig. 4b). NO_3^-–N loading during the dry season only accounted for a small proportion of the total annual loading at two headwater catchments (CHQ and CC), and the surface river HZ-R (max 9.0%) but was a greater contribution of annual NO_3^-–N export at LHT and MSK (max 39.4%) (Table 1).

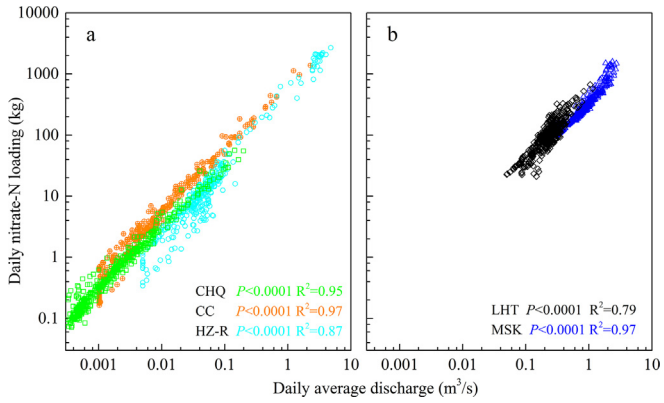

Fig. 3. Relationships between nitrate-N daily loading and daily average discharge measured by the in-situ sensors at (a) CHQ, CC and HZ-R; (b) LHT and MSK.

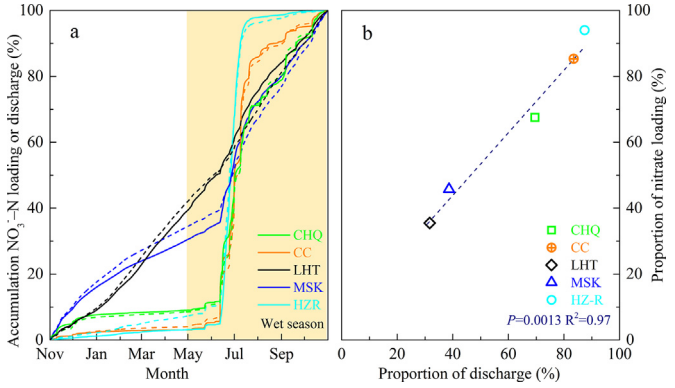

Fig. 4. (a) The relationship between cumulative NO_3^-–N loading and discharge within Houzhai Catchment. The straight and dash lines with same color represent cumulative NO_3^-–N loading and discharge at same site, respectively. (b) The relationship between proportion of discharge and nitrate loading for June to August 2017, the period of greatest change in fluvial loading.

It is important to consider how the amount of NO_3^-–N exported relates to catchment drainage size, as land use can be more diverse in larger catchments. Thus, we explored how export differs across the catchments when normalized for surface area - noting we assume that all catchments have a similar density and reach of underground flow networks, and this may not be the case (Hartmann et al., 2014). Total normalized export for one year 2016–2017 ranged from 7.0 ± 1.4 (CHQ) to 30.2 ± 2.4 kg/ha (CC), with the lowest and highest loading found in the headwater catchments. The normalized annual loading generally decreases with increasing catchment size (Table 1), the exception being CHQ which has the lowest normalized export and is the catchment with the least farmland and most natural vegetation. In comparison during event flow, surface run-off generates flow in the channel at CC, but not at CHQ.

Slight decreases in export with increasing catchment size are apparent when only area used for agriculture is used to calculate the loading. However, total nitrate export from Houzhai comprises both the upwelling underground stream (MSK) and the HZ-river export, and thus total export from the Houzhai Catchment (MSK and HZ-R) for one year from November 2016 to October 2017 is 22.2 kg/ha, and 54.1 kg/ha if normalized for only agricultural area (Table 1). The percentage of land surface that is farmland in each catchment increases with size which would be expected to increase loading to catchment drainage, yet the loading decreases. This indicates that net nitrate consumption or storage is taking place within the catchment, as a result of biological activity, spatial variation of nitrate export, or within the reservoir, which takes surface flow from the northern drainage channels, by denitrification and assimilation (Heffernan et al., 2012; Rode et al., 2016).

The use of in-situ nitrate sensors is not routine, so there are limited other catchment studies for comparison and not for the same hydrological year. Of those that exist, the normalized NO_3^-–N export from the small Houzhai karst catchment is greater than larger or similar sized catchments that do not contain karst (Jacobs et al., 2018; Miller et al., 2016; Outram et al., 2016), and less than larger catchment that do contain karst with more farmland (Table S5) (Hansen and Singh, 2018; Jones et al., 2018). Thus it appears that the combination of farmland (high nitrogen availability), hydrological pattern and hydrogeological structure in KCZ leads to increased nitrate mobilization and transport to drainage (Fig. S4) with the karst doing little store or attenuate nitrate in KCZ, with rapid transported event flow during high sources availability periods would concentrate nitrate export into a couple of months.

3.3. Land use and hydrological interaction

We have a complete [NO_3^-–N] time series for the wet season in 2017 and so can consider in detail changes during event flow. During the

early wet season, with dry conditions from May to the onset of event No. 4 in the middle of June, Q was generally unresponsive to the low-level rainfall and groundwater abstraction for irrigation was ongoing. However, [NO_3^-–N] showed increases during these small events to concentrations comparable with, or even greater than, the largest hydrological events later in the wet season. Hydrological models for this catchment suggest that baseflow is maintained by slow flow pathways of longer residence time (Zhang et al., 2019), and these are unlikely to represent a highly mobile nitrate reservoir.

Thus, to observe an increase in concentration in response to small increases in flow suggests these small events are mobilizing nitrate stored locally and only transported when the surface receives rainfall (as otherwise nitrate could be consumed during transport). This points to the soil as the source of this local and responsive reservoir. During dry conditions, there will be reduced biological nitrate uptake due to limited plant growth, and conversion of NH_4^+ absorbed in the soil to inorganic N by mineralization (organic N → NH_4^+) and nitrification (NH_4^+ → NO_3^-) (Krause et al., 2015; Lawler et al., 2006; Ouyang et al., 2015). With rainfall comes a flushing effect: nitrate is mobilized from soils which have experienced a long period of dry conditions (Blaen et al., 2017). Additionally, agricultural practices, e.g. tillage, artificial irrigation and associated fertilization, are intensive during the early part of wet season (Fig. 2), all of which can accumulate NO_3^-–N in epikarst (Chen et al., 2017; Pellerin et al., 2014; Schilling and Zhang, 2004). Despite less rainfall and lower Q during the early wet season, accumulated NO_3^-–N can leach to underground streams, such that rainfall mobilized NO_3^-–N in the epikarst causes a rapid increase of [NO_3^-–N] despite relatively low Q at all sites.

The frequent and heavy rain after the middle of June (event 4) was sufficient to recharge and initiate a sustained hydrological response allowing for more saturated conditions across the catchment (Fig. 2). The repeated higher concentration of [NO_3^-–N] after fertilizer application suggests that nitrate availability may be a stronger driver of loss to drainage than hydrological activity (Huebsch et al., 2014; Opsahl et al., 2017). The [NO_3^-–N] during events in the later wet season was generally less than the early wet season, and the concentration in the headwater catchments (CHQ, CC) returned to pre-event values more quickly. However, the opposite was observed with the underground streams at the larger catchment scale (LHT, MSK) and in the surface water (HZ-R) (Fig. 1a). More land is used for rice paddies and settlements in LHT and MSK than the CC and CHQ headwater catchments (Fig. 1b) and these areas could act as reservoirs for nitrate release resulting in a prolonged release of nitrate (evident in broader concentration event profiles) (Ouyang et al., 2015).

As the catchment becomes wetter and close to saturation, there is greater hydrological connectivity to increase the drainage area (Chen et al., 2018; Peng and Wang, 2012), and more nitrate is produced as soils become wetter and bacterial processes can be enhanced (Hansen and Singh, 2018). Therefore, there is more nitrate available to be leached and more nitrate-rice water in saturated fissures. Successive rainfall events can then facilitate this leaching (Rusjan et al., 2008), particularly during the fertilization-application period.

Additionally, the flow pathway changes to conduit flow from overland flow and runoff with low [NO_3^-–N] but high loading, which can be observed in accumulation loading and discharge patterns (Fig. 4a). The slopes differ in Fig. 4a across the catchment with headwater sites CHQ and CC showing steep cumulative export of NO_3^-–N in the mid-wet season, but the rate of export decreases in the late wet season, suggesting nitrate leaching is slowing down as the sources are depleted. Thus, the interaction of nitrogen source availability and fast response karstic hydrology during the wet season results in the dynamic cumulative export of NO_3^-–N.

3.4. Nitrate reservoir mobilization varies across the karst system

Hydrological modelling suggests that infiltrated water quickly fills conduits where the water table is higher than the adjacent fractures or fissures, especially during the wet season with event flows, which result in water temporarily stored in the conduits recharging the fractures or fissures (Sorensen et al., 2015; Zhang et al., 2017). The total ranges in [NO_3^-–N] during the early phase of the wet season were quite similar between the three sites in the upper to mid-catchment: CHQ (1.9–10.2 mg/L), CC (1.7–12.5 mg/L), LHT (4.5–12.2 mg/L). These ranges were larger than MSK (3.7–6.3 mg/L) and HZ-R (0.7–5.6 mg/L), which could indicate attenuation of nitrate during transit or dilution, or only partial export from a local area to the outlet such that concentration decreases (Chen et al., 2018; McMahon and Bolke, 2006). During the mid-wet season, unlike CHQ and CC, [NO_3^-–N] at LHT still increases quickly in response to event flow (Events 7 and 8), and it appears that the concentration decreases more slowly post-event (peak broadening, 0.17 and 0.02 mg/L/h, respectively). These patterns suggest two sources of nitrate: release from that stored in the fissures and conduits, and transport from the surface soils. This pattern may be apparent at LHT and not CC and CHQ as the karst underground network is more developed at LHT.

At MSK, the event concentration is higher but decreases with time despite successive events suggesting depletion of nitrate stores. The slope of LHT and MSK in Fig. 4 showed steady and more linear export of NO_3^-–N and suggested a greater contribution from NO_3^-–N stored in the karst aquifer system and exported more slowly. At HZ-R, the maximum [NO_3^-–N] occurred much later than the other sites, likely reflecting a lag induced due to the reservoir initially storing and later releasing run-off. Cumulative NO_3^-–N export for HZ-R is similar to CHQ and CC as HZ-R is regulated by the QS-Re and so discharge increases in the wet season as the reservoir refills and overspills and brings NO_3^-–N.

Sometimes, similar to LHT, there were sharp increases in [NO_3^-–N] at some of sites and across the dry and wet season. These probably reflect a localized source input particularly in areas of developed land use as the N loading from anthropological input (sewage and manure) with high [NO_3^-–N] from daily life is not seasonally variable.

3.5. How the karst critical zone influences fluvial NO_3^-–N export and water quality

The hydrological functioning of this karst system can be described as follows. Water stored in the karst matrix maintains base flow in the wet season and becomes a more important reservoir for discharge in the dry season, with increased aquifer saturation increasing transmissivity and recharging the aquifer in advance of the dry season. The water that recharges the aquifer comes from hillslope flow, of which the surface run-off component is small and most water goes into the karst aquifer system. However, in the valley depression surface run-off as fast flow is more important and can drain directly into sinkholes or from soils into the underlying epikarst. This contribution also recharges the aquifer introducing nitrate to the matrix, which unless denitrified, can be released later through slower flow pathways (Chen et al., 2018; Fu et al., 2016; Sorensen et al., 2015).

Maximal nitrate event flow concentration generally lags peak Q, which indicates first water low in nitrate (high-slope recharge) is discharged and then waters with greater nitrate concentration become increasingly important. As a typical geomorphology in karst area, SW china, peak clusters form more hillslope area (Liu et al., 2004). Forest and shrubs predominate the hillslope areas (a major land use, Table S1), but the nitrate concentration here is low, generally <1 mg/L [NO_3^-–N] most likely from atmospheric deposition (Xiao et al., 2013). Clearly this cannot account for the concentration time series, which is always >1 mg/L, and up to 16.3 mg/L. Mixing with lower concentration hillslope waters, the concentration can be up to the mean value of 5.5 mg/L. The variability of nitrate in event flow reflects mixing of the hillslope waters with valley bottom waters. In turn this reflects antecedent saturation of the epikarst and the underlying aquifer, as this influence whether rainfall penetrates the epikarst or forms surface run-off. Thus, the valley bottom drainage is an important source of nitrate to

the karst aquifer, with sufficient nitrate from farmed soils. The accelerating nitrate concentration profile associated with event flow indicates that the valley bottom waters continue to contribute nitrate to the aquifer as Q subsides.

In the lower catchment the land surface is flatter and most of the water is considered to move through fractures in the aquifer matrix i.e. drainage capacity decreases and storage capacity increases (Zhang et al., 2016). Increasing fracture transmission increases the important of slow flow in the network, reflecting in NO_3^-–N event pattern less sensitive to rainfall events and high proportion of the total annual NO_3^-–N loading during dry season (e.g., compare MSK and LHT).

Additionally, there is likely to be temporal variability in valley bottom nitrate availability depending on agricultural driven changes in land management. As agricultural practices are less intense and rainfall-driven event flow generally absent, the relative constancy in [NO_3^-–N] suggests on-going release of nitrate, stored close to slow flow pathways (fissures). This is evidenced by constancy in baseflow nitrate concentrations between events, across seasons and across sites, and thus could be considered to represent chronic aquifer nitrate pollution with old waters recharged by new waters that have more nitrate.

Although there is chronic aquifer nitrate pollution, [NO_3^-–N] during most of study period are below the China drinking water standard threshold of 10 mg/L (MOH and SAC, 2006). Only rarely do sites have [NO_3^-–N] higher than this threshold, e.g. 0.11% of time at CHQ, 2.34% at CC, 0.90% at LHT-S and 0.06% at HZ-R. However, for 83% of the time [NO_3^-–N] at HZ-R exceeded the Chinese Environmental Quality Standards for Surface Water quality (criterion V, 2 mg/L as TN) (SEPAC, 2002) and all upwelling underground streams, which contribute to surface flow on emergence, exceeded this standard for the duration of study. This consideration is not unique to karst systems. However, karst systems with their dependence on conduit flow and potential for high transmissivity, may also offer a hydrologically responsive setting to reduce nitrate loading through precision-farming approaches (Jin et al., 2017; Zhang et al., 2015).

4. Conclusion

Using sensor technology to understand nitrate dynamics in this karst system has revealed that i) there is chronic aquifer nitrate pollution, ii) nitrate is lost to catchment drainage and then transported within the karst through the catchment, iii) the timing of nitrate loss is dependent on the interaction of land use, hydrology and karst architecture. Most NO_3^-–N is exported in the wet season (e.g. CHQ, CC) when nitrate used in agriculture is not retained, with this lack of retention 'fueling' the export. Where NO_3^-–N is exported more steadily it is because catchment drainage is accessing epikarst NO_3^-–N storage (e.g. MSK, LHT). Thus, to reduce aquifer pollution, and to stop the downstream drainage system receiving excess nitrate, changes to land management practices should be considered. Our research suggests that NO_3^-–N reduction efforts should be targeted at identifying appropriate control strategies for reconciling the timing of fertilizer applications and crop requirement, to reduce NO_3^-–N losses within the field before downstream transport. The effectiveness of this could be assessed by on-going sensor monitoring to detect a reduction in base flow concentration, providing evidence of effective land management strategies for policy makers and catchment managers of karst agricultural areas.

Acknowledgments

The authors would like to acknowledge funding from the Natural Environment Research Council, United Kingdom, Grant/Award Number: NE/N007425/1 and the National Natural Science Foundation of China, China, Grant/Award Number: 41571130072. We thank Drs Cai-Qing Qin, Yu-Chong Fu for their help in sensor installation and data collection. F-JY, SW, S-LL and DO designed the research objectives and interpreted the data and prepared the manuscript. FJY, ZJW, JZ and SX carried out the field and laboratory work. Z-CZ aided the hydrological interpretation and interpreted the hydrological knowledge. All of authors participated in discussion of the results.

Declaration of competing interest

The authors declare no competing financial interests.

Appendix A. Supplementary data

Supplementary data to this article can be found online at https://doi.org/10.1016/j.scitotenv.2019.134062.

References

Bai, Z.H., Zhao, H., Velthof, G.L., Oenema, O., Chadwick, D., Williams, J.R., Jin, S.Q., Liu, H.B., Wang, M.R., Strokal, M., Kroeze, C., Hu, C.S., Ma, L., 2018. Designing vulnerable zones of nitrogen and phosphorus transfers to control water pollution in China. Environ. Sci. Technol. 52 (16), 8987–8988.

Blaen, P.J., Khamis, K., Lloyd, C.E.M., Bradley, C., Hannah, D., Krause, S., 2016. Real-time monitoring of nutrients and dissolved organic matter in rivers: capturing event dynamics, technological opportunities and future directions. Sci. Total Environ. 569, 647–660.

Blaen, P.J., Khamis, K., Lloyd, C., Comer-Warner, S., Ciocca, F., Thomas, R.M., MacKenzie, A.R., Krause, S., 2017. High-frequency monitoring of catchment nutrient exports reveals highly variable storm event responses and dynamic source zone activation. J. Geophys. Res.-Biogeo. 122 (9), 2265–2281.

Buckerfield, S.J., Waldron, S., Quilliam, R.S., Naylor, L., Li, S.L., Oliver, D.M., 2019. How can we improve understanding of faecal indicator dynamics in karst systems under changing climatic, population, and land use stressors?–Research opportunities in SW China. Sci. Total Environ. 646, 438–447.

Chen, H.Y., Chen, X.Y., Chen, B., 2005. Study on hydrological characteristics of Houzhai karst small valley, Puding. Guizhou Province. Guizhou Geology 22, 284–288 (In Chinese with English Abstract).

Chen, J., Xiao, G.L., Kuzyakov, Y.K., Jenerette, G.D., Ma, Y., Liu, W., Wang, Z., Shen, W., 2017. Soil nitrogen transformation responses to seasonal precipitation changes are regulated by changes in functional microbial abundance in a subtropical forest. Biogeosciences 14, 2513–2525.

Chen, X., Zhang, Z.C., Soulsby, C., Cheng, Q.B., Binley, A., Jiang, R., Tao, M., 2018. Characterizing the heterogeneity of karst critical zone and its hydrological function: an integrated approach. Hydrol. Process. 32 (19), 2932–2946.

Coxon, C., 2011. Agriculture and Karst. In: van Beynen, P. (Ed.), Karst Management. Springer, pp. 103–138.

Einsiedl, F., Mayer, B., 2006. Hydrodynamic and microbial processes controlling nitrate in a fissured-porous karst aquifer of the Franconian Alb, Southern Germany. Environ. Sci. Technol. 40 (21), 6697–6702.

Einsiedl, F., Maloszewski, P., Stichler, W., 2009. Multiple isotope approach to the determination of the natural attenuation potential of a high-alpine karst system. J.Hydrol. 365 (1–2), 113–121.

Exner-Kittridge, M., Strauss, P., Bloschl, G., Eder, A., Saracevic, E., Zessner, M., 2016. The seasonal dynamics of the stream sources and input flow paths of water and nitrogen of an Austrian headwater agricultural catchment. Sci. Total Environ. 542, 935–945.

Feng, Y.H., Song, B., Fan, W.G., Zhou, W.J., Pan, X.S., Tian, J.W., 2009. The technical regulations of tillage transplanting for rich production. Guizhou Province. Till. Cultiv. 3, 54–60 (In Chinese).

Fenton, O., Mellander, P.E., Daly, K., Wall, D.P., Jahangir, M.M.R., Jordan, P., Hennessey, D., Huebsch, M., Blum, P., Vero, S., Richard, K.G., 2017. Integrated assessment of agricultural nutrient pressures and legacies in karst landscapes. Agric. Ecosyst. Environ. 239, 246–256.

Ford, D., Williams, P.D., 2013. Karst Hydrogeology and Geomorphology. John Wiley & Sons.

Fu, T.G., Chen, H.S., Wang, K.L., 2016. Structure and water storage capacity of a small karst aquifer based on stream discharge in southwest China. J. Hydrol. 534, 50–62.

Hansen, A., Singh, A., 2018. High frequency sensor data reveal across-scale nitrate dynamics in response to hydrology and biogeochemistry in intensively managed agricultural basins. J. Geophys. Res.-Biogeo. 123, 2168–2182.

Hartmann, A., Goldscheider, N., Wagener, T., Lange, J., Weiler, M., 2014. Karst water resources in a changing world: review of hydrological modeling approaches. Rev. Geophys. 52 (3), 218–242.

Heffernan, J.B., Albertin, A.R., Fork, M.L., Katz, B.G., Cohen, M.J., 2012. Denitrification and inference of nitrogen sources in the karstic Floridan Aquifer. Biogeosciences 9 (5), 1671–1690.

Huebsch, M., Fenton, O., Horan, B., Hennessy, D., Richards, K.G., Jordan, P., Goldscheider, N., Butscher, C., Blum, P., 2014. Mobilisation or dilution? Nitrate response of karst springs to high rainfall events. Hydrol. Earth Syst. Sci. 18 (11), 4423–4435.

Jacobs, S.R., Weeser, B., Guzha, A.C., Rufino, M.C., Butterbach-Bahl, K., Windhorst, D., Breuer, L., 2018. Using high-resolution data to assess land use impact on nitrate dynamics in East African tropical montane catchments. Water Resour. Res. 54 (3), 1812–1830.

Jiang, Y.J., Wu, Y.X., Yuan, D.X., 2009. Human impacts on karst groundwater contamination deduced by coupled nitrogen with strontium isotopes in the Nandong underground river system in Yunan, China. Environ. Sci. Technol. 43 (20), 7676–7683.
Jin, Z., Prasad, R., Shriver, J., Zhuang, Q., 2017. Crop model-and satellite imagery-based recommendation tool for variable rate N fertilizer application for the US Corn system. Precis. Agric. 18 (5), 779–800.
Jones, C.S., Davis, C.A., Drake, C.W., Schilling, K.E., Debionne, S.H.P., Gilles, D.W., Demir, I., Weber, L.J., 2018. Iowa statewide stream nitrate load calculated using in situ sensor network. J.Am. Water Resour. As. 54 (2), 471–486.
Jost, G., Dirnbock, T., Grabner, M.T., Mirtl, M., 2011. Nitrogen leaching of two forest ecosystems in a karst watershed. Water Air Soil Poll 218 (1–4), 633–649.
Katz, B.G., Bohlke, J.K., Hornsby, H.D., 2001. Timescales for nitrate contamination of spring waters, northern Florida, USA. Chem. Geol. 179 (1–4), 167–186.
Krause, S., Lewandowski, J., Dahm, C.N., Tockner, K., 2015. Frontiers in real-time ecohydrology - a paradigm shift in understanding complex environmental systems. Ecohydrology 8 (4), 529–537.
Lassaletta, L., Billen, G., Grizzetti, B., Garnier, J., Leach, A.M., Galloway, J.N., 2014. Food and feed trade as a driver in the global nitrogen cycle: 50-year trends. Biogeochemistry 118 (1–3), 225–241.
Lawler, D.M., Petts, G.E., Foster, I.D.L., Harper, S., 2006. Turbidity dynamics during spring storm events in an urban headwater river system: the upper tame, west midlands, UK. Sci. Total Environ. 360 (1–3), 109–126.
Liu, Z.H., Groves, C., Yuan, D.X., Meiman, J., 2004. South China karst aquifer storm-scale hydrochemistry. Ground Water 42 (4), 491–499.
Liu, C.Q., Li, S.L., Lang, Y.C., Xiao, H.Y., 2006. Using $\delta^{15}N$ and delta $\delta^{18}O$ values to identify nitrate sources in karst ground water, Guiyang, Southwest China. Environ. Sci. Technol. 40 (22), 6928–6933.
Liu, C.C., Liu, Y.G., Guo, K., Wang, S.J., Liu, H.M., Zhao, H.W., Qiao, X.G., Hou, D.J., Li, S.B., 2016. Aboveground carbon stock, allocation and sequestration potential during vegetation recovery in the karst region of southwestern China: a case study at a watershed scale. Agric. Ecosyst. Environ. 235, 91–100.
McCormack, T., Naughton, O., Johnston, P.M., Gill, L.W., 2016. Quantifying the influence of surface water-groundwater interaction on nutrient flux in a lowland karst catchment. Hydrol. Earth Syst. Sci. 20 (5), 2119–2133.
McMahon, P.B., Bolke, J.K., 2006. Regional patterns in the isotopic composition of natural and anthropogenic nitrate in groundwater, high plains, USA. Environ. Sci. Technol. 40 (9), 2965–2970.
Miller, M.P., Tesoriero, A.J., Capel, P.D., Pellerin, B.A., Hyer, K.E., Burns, D.A., 2016. Quantifying watershed-scale groundwater loading and in-stream fate of nitrate using high-frequency water quality data. Water Resour. Res. 52 (1), 330–347.
Ministry of Health of the People's republic of China & Standardization Adminstration of P.R. China MOH & SAC, 2006. Chinese National Standards GB 5749–2006: Standards for Drinking Water Quality. Standards Press of China.
Musgrove, M., Opsahl, S.P., Mahler, B.J., Herrington, C., Sample, T.L., Banta, J.R., 2016. Source, variability, and transformation of nitrate in a regional karst aquifer: Edwards aquifer, central Texas. Sci. Total Environ. 568, 457–469.
Opsahl, S.P., Musgrove, M., Slattery, R.N., 2017. New insights into nitrate dynamics in a karst groundwater system gained from in situ high-frequency optical sensor measurements. J. Hydrol. 546, 179–188.
Outram, F.N., Cooper, R.J., Sunnenberg, G., Hiscock, K.M., Lovett, A.A., 2016. Antecedent conditions, hydrological connectivity and anthropogenic inputs: factors affecting nitrate and phosphorus transfers to agricultural headwater streams. Sci. Total Environ. 545, 184–199.
Ouyang, W., Chen, S.Y., Wang, X.L., Shan, Y.S., 2015. Paddy rice ecohydrology pattern and influence on nitrogen dynamics in middle-to-high latitude area. J. Hydro. 529, 1901–1908.
Pellerin, B.A., Saraceno, J.F., Shanley, J.B., Sebestyen, S.D., Aiken, G.R., Wollheim, W.M., Bergamaschi, B.A., 2012. Taking the pulse of snowmelt: in situ sensors reveal seasonal, event and diurnal patterns of nitrate and dissolved organic matter variability in an upland forest stream. Biogeochemistry 108 (1–3), 183–198.
Pellerin, B.A., Bergamaschi, B.A., Gilliom, R.J., Crawford, C.G., Saraceno, J., Frederick, C.P., Downing, B.D., Murphy, J.C., 2014. Mississippi River nitrate loads from high frequency sensor measurements and regression-based load estimation. Environ. Sci. Technol. 48 (21), 12612–12619.
Peng, T., Wang, S.J., 2012. Effects of land use, land cover and rainfall regimes on the surface runoff and soil loss on karst slopes in southwest China. Catena 90, 53–62.
Pu, J.B., Yuan, D.X., He, Q.F., Wang, Z.J., Hu, Z.Y., Gou, P.F., 2011. High-resolution monitoring of nitrate variations in a typical subterranean karst stream, Chongqing, China. Environ. Earth Sci. 64 (7), 1985–1993.
Rode, M., Angelstein, S.H.N., Anis, M.R., Borchardt, D., Weitere, M., 2016. Continuous in-stream assimilatory nitrate uptake from high frequency sensor measurements. Environ. Sci. Technol. 50 (11), 5685–5694.
Rusjan, S., Brilly, M., Mikos, M., 2008. Flushing of nitrate from a forested watershed: an insight into hydrological nitrate mobilization mechanisms through seasonal high-frequency stream nitrate dynamics. J. Hydrol. 354 (1–4), 187–202.
Schilling, K., Zhang, Y.K., 2004. Baseflow contribution to nitrate-nitrogen export from a large, agricultural watershed, USA. J. Hydrol. 295 (1–4), 305–316.
Shore, M., Jordan, P., Melland, A.R., Mellander, P.E., McDonald, N., Shortle, G., 2016. Incidental nutrient transfers: assessing critical times in agricultural catchments using high-resolution data. Sci. Total Environ. 553, 404–415.
Sorensen, J.P.R., Butcher, A.S., Stuart, M.E., Townsend, B.R., 2015. Nitrate fluctuations at the water table: implications for recharge processes and solute transport in the Chalk aquifer. Hydrol. Process. 29 (15), 3355–3367.
State Environmental Protection Administration of China-SEPAC, 2002. Environmental Protection Agency and General Administration of Quality Supervision, Inspection and Quarantine of China. GB383822002 Environmental Quality Standards for Surface Water. China Environmental Sicence Press, Beijing.
Tang, W.Z., Ping, J.F., Fan, K., Wang, Y.X., Luo, X., Ying, Y.B., Wu, J., Zhou, Q.L., 2012. All-solid-state nitrate-selective electrode and its application in drinking water. Electrochim. Acta 81, 186–190.
Van Meter, K.J., Basu, N.B., Van Cappellen, P., 2017. Two centuries of nitrogen dynamics: legacy sources and sinks in the Mississippi and Susquehanna River Basins. Global Biogeochem. Cy. 31 (1), 2–23.
Wang, L., Zhang, Y., 2001. Karst conduit flow and its hydrodynamic characteristics—Houzhai River drainage basin in Puding, Guizhou, China as an example. Chin. Sci. Bull. 46 (1), 45–50.
Wymore, A.S., Coble, A.A., Rodríguez-Cardona, B., McDowell, W.H., 2016. Nitrate uptake across biomes and the influence of elemental stoichiometry: a new look at LINX II. Global Biogeochem. Cy. 30 (8), 1183–1191.
Xiao, H.W., Xiao, H.Y., Long, A.M., Wang, Y.L., Liu, C.Q., 2013. Chemical composition and source apportionment of rainwater at Guiyang, SW China. J. Atmos. Chem. 70 (3), 269–281.
Yang, L.Z., 1981. The characteristics of underground flow in Houzhai Catchment, Puding, Guizhou Province. Jounal of Chengdu College of Geology 01, 77–85 (In Chinese).
Yue, F.-J., Li, S.-L., Zhong, J., Liu, J., 2018. Evaluation of factors driving seasonal nitrate variations in surface and underground systems of a Karst Catchment. Vadose Zone J. 17 (1).
Zhang, X., Davidson, E.A., Mauzerall, D.L., Searchinger, T.D., Dumas, P., Shen, Y., 2015. Managing nitrogen for sustainable development. Nature 528 (7580), 51.
Zhang, R.R., Shu, L.C., Zhu, J.T., Yu, Z.B., Jiang, P., 2016. Storage and drainage characteristics of a highly heterogeneous karst aquifer in Houzhai Basin. Groundwater 54 (6), 878–887.
Zhang, Z.C., Chen, X., Soulsby, C., 2017. Catchment-scale conceptual modelling of water and solute transport in the dual flow system of the karst critical zone. Hydrol. Process. 31 (19), 3421–3436.
Zhang, Z., Chen, X., Cheng, Q., Soulsby, C., 2019. Storage dynamics, hydrological connectivity and flux ages in a karst catchment: conceptual modelling using stable isotopes. Hydrol. Earth Syst. Sci. 23 (1), 51–71.